29th Congress of the International Council
of the Aeronautical Sciences
St. Petersburg, Russia; September 7–12, 2014

# FLIGHT ENVELOPE EXPANSION VIA ACTIVE CONTROL SOLUTIONS FOR A GENERIC TAILLESS AIRCRAFT

**N. Abramov* , M. Bommanahal** , S. Chetty** , M. Goman* , E. Kolesnikov* , PVS. Murthy****
***De Montfort University, UK, **CSIR-National Aerospace Laboratories, Bangalore, India**

**Keywords:** *flight envelope expansion, HAoA modeling, attainable equilibrium sets, command stability augmentation system, regions of attraction, wing-rock, spin, numerical simulation*

## Abstract

*Aircraft dynamics at high angles of attack due to loss of stability and control essentially limits its manoeuvrability. Modern control systems implement flight envelope protection at the cost of maneuverability to improve safety in these conditions. Flight envelope boundaries, which are set taking into account deterioration of stability and controllability due to separated flow, can be expanded by appropriate design of control laws. However, such a design requires extensive analysis of the maneuver envelope of the airframe and its utilization by the flight envelope protection laws. The reliability of this analysis depends on the adequate aerodynamic modeling which captures nonlinear unsteady variation of aerodynamic loads in these flight regimes. Two novel models for unsteady aerodynamics at low and high subsonic Mach numbers are described. These models and prototyping control laws are used for closed loop computational analysis. The computational methodology of clearing flight control laws for flight envelope expansion of a Generic Tailless Aircraft (GTA) is addressed.*

## 1 Introduction

Flight safety of military and commercial transport aircraft is directly connected with their behaviour at high angles of attack and reliability of its flight envelope protection. Expansion of flight envelope leads to increase in manoeuvrability of military aircraft, while effective flight envelope protection helps to avoid loss-of-control in flight (LOC-I) for civil transport aircraft [1]. The results obtained during the collaborative research project between CSIR-NAL, India and De Montfort University (DMU) highlight the main problems and limitations in expansion of GTA flight envelope. We performed evaluation of prototype control laws with objective of their redesign for extension of flight envelope. This paper presents the employed methodology and computational framework developed earlier at DMU with some preliminary results and analysis.

A number of methodological challenges were addressed and effectively implemented for finding feasible solutions to the formulated objective. Firstly, the methods for adequate modeling of GTA aerodynamics in the extended flight envelope to capture unsteady variation of coefficients due to separated flow, vortex breakdown, onset of aerodynamic asymmetry, etc. were developed [1, 5, 6, 7, 8, 9]. These models were augmented to the classical aerodynamic database. Secondly, a systematic investigation of GTA nonlinear dynamics to characterize its critical flight regimes in the extended envelope for the airframe was conducted. This provided a clear understanding of GTA's susceptibility to lateral-directional loss of control, behaviour in wing rock and spin modes, etc. [11, 12, 13]. Thirdly, the clearance of flight control laws in the extended flight envelope based on computation of attainable equilibrium sets and regions of attraction for GTA with command and stability augmentation system has been effectively implemented [14].

Based on deep insights into the problems gained at this stage, it is anticipated that the de-

sign of efficient control laws for extended flight envelope will be a success. The developed computational framework will be used and adjusted for this purpose.

## 2 Aerodynamic Modeling in the Extended Flight Envelope

The flight envelope Of Mach versus $\alpha$ is restricted at two boundaries due to deterioration in aerodynamics. At one boundary there is vortex-breakdown on wings and at the other boundary there is asymmetric shock induced flow separation on the wings. These phenomena result in unsteady and nonlinear variation of aerodynamic loads [3, 5, 7]. Traditional methods of wind tunnel tests and aerodynamic models are insufficient for formulating flight control and testing strategies. Therefore, aerodynamic modeling for these flight conditions has been pursued for the past two decades. In this section, we present novel models for these phenomena in the form of nonlinear differential equations.

Both these models were developed for GTA using experimental data from industrial grade wind tunnels. These were easily integrated to classical data-table aero-models for the purpose of real-time simulation and off-line flight dynamic analysis.

### 2.1 Modeling High-angle-of-attack unsteady aerodynamics

At low-speed, high angle-of-attack flight conditions the delta wing aerodynamics is dominated by vortex flow on the wing. This vortex flow readjusts to change in external flow conditions, that is $\alpha$ and $\beta$, with a certain time-lag. This has been observed in flow visualization studies and dynamic wind tunnel test data. This causes the variation in aerodynamic forces and moments in a dynamic maneuver to be significantly different from that obtained from aero-database. This does not alter the possible aircraft trims, but affects dynamics and local stability characteristics.

Modeling the unsteady variation in aerodynamic forces and moments requires special experimental data and mathematical system identi-

fication techniques, like that in [5, 7]. Classically wind tunnel test response of aerodynamic coefficients obtained by forced oscillations in pitch, roll and yaw for various amplitude and frequency inputs are used for modeling this phenomena. We present a Volterra variational equations based model that can be estimated using forced oscillation test data [4, 8]. It can also be used for estimation using flight test data or other dynamic tests like the ones done on a 5DOF rig [10].

Forced oscillation wind tunnel test data showed that the variation in coefficients is nonlinear for large amplitude and linear for small amplitude sinusoidal alpha input. Also, the damping derivatives estimated from small amplitude forced oscillation wind tunnel test data are strong functions of frequency. All these effects are captured by a single model structure presented here.

The normal force dependence on angle-of-attack in static conditions be given by $Cz_{st}(\alpha)$, and the increment over it due to unsteady aerodynamics be $C_d(t)$, then variation of normal force $Cz(t)$ in a maneuver is,

$$Cz(\alpha(t),t) = Cz_{st}(t) + Cz_q(t) \cdot q\bar{c}/2V + C_d(t) \quad (1)$$

We model $C_d(\dot{\alpha}(t))$ in the from of Volterra variational equations. This system has a stable equilibrium point $[C_d(t), \dot{\alpha}(t)) = (0,0)]$ for the entire $\alpha \in [-90^o, 90^o)$ range. For model structure of Eq.(1), $Cz(t)$ converges to $Cz_{st}$ in a finite time when $(\dot{\alpha} = 0)$. The nonlinear model for $C_d(t)$ in the form of Volterra-variational equations is given by Eq.(2).

$$\begin{aligned} C_d(t) &= x_1(t) + x_2(t) + x_3(t) \\ \dot{x}_1(t) &= a(\alpha(t))x_1(t) + K_1(\alpha(t))\dot{\alpha}(t), \; x_1(0) = 0 \\ \dot{x}_2(t) &= a(\alpha(t))x_2(t) + K_{20}(\alpha(t))x_1^2(t) + \quad (2) \\ &\quad K_{21}(\alpha(t))x_1(t)\dot{\alpha}(t), \; x_2(0) = 0 \end{aligned}$$

In this structure, first kernel state $x_1$ indicates the linear response of unsteady aerodynamics to $\dot{\alpha}(t)$, with $a$ as time-scale parameter. The magnitude of $x_2$ is likely to be significant when there is large amplitude change in $\alpha$ or $\dot{\alpha}$, and it produces second harmonic component in response to sinusoidal input.

In a small amplitude forced oscillation test, wind tunnel model is oscillated in pitch in
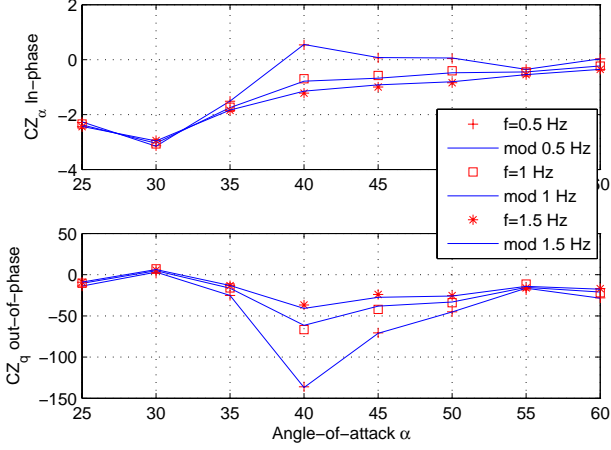
**Fig. 1** Comparison of the in-phase and out-of-phase aerodynamic derivatives predicted by aerodynamic model and extracted from experimental data for Cz of GTA.



**Fig. 2** Comparison of predicted and experimental aerodynamic responses for Cz of GTA.

a sinusoidal motion given by, $\alpha_{exp}(t) = \alpha_0 + \Delta\alpha \sin(\omega t)$. The measured normal force coefficient $Cz(t)$ is converted to in-phase derivative $Cz_\alpha(\alpha_0)$ and out-of-phase derivative $Cz_{\dot\alpha}(\alpha_0)$ by harmonic analysis of the time-series data. Therefore, the steady-state response of the normal force coefficient is given by,

$$Cz(t) = Cz_0(\alpha_0) + Cz_{\alpha,\omega_0}(\alpha_0)\Delta\alpha \sin(\omega t) + \quad (3)$$
$$Cz_{\dot\alpha,\omega_0}(\alpha_0)\frac{\omega\bar{c}}{2V}\Delta\alpha\cos(\omega t)$$

Since small amplitude data shows linear variation of $Cz(t)$, we consider only first kernel state in $C_d(t)$. For parameter estimation using this data we linearize the model in Eq.(2), and get its steady state response to $\alpha_{exp}(t)$ as,

$$Cz(t)_{ss} = \left[Cz_{\alpha,st}(\alpha_0) + \frac{K_1\omega^2}{a^2+\omega^2}\right]\Delta\alpha\sin(\omega t) \quad (4)$$
$$\left[-\frac{K_1a}{a^2+\omega^2}\frac{\bar{c}\omega}{2V} + Cz_q(\alpha_0)\frac{\omega\bar{c}}{2V}\right]\Delta\alpha\cos(\omega t)$$

Comparing Eq.(4) and Eq.(3), we get the following relation between experimental derivatives and model parameters,

$$Cz_{\alpha,\omega_0}(\alpha_0) = Cz_{\alpha,st}(\alpha_0) + \frac{K_1\omega^2}{a^2+\omega^2}$$
$$Cz_{\dot\alpha,\omega_0}(\alpha_0) = Cz_q(\alpha_0) - \frac{K_1a}{a^2+\omega^2} \quad (5)$$

Rearranging the terms in Eq.(5), we get a linear relation between $Cz_{\alpha,\omega_0}(\alpha_0)$ and $Cz_{q,\omega_0}(\alpha_0)$. This relation is used in a two-step regression as proposed in [9], to obtain estimate of parameters $(a, K1)$ at each $\alpha_0$ for which data is available. The model matches the experimental data consistently as shown in Fig. 1.

The nonlinear variation can be captured by considering the second kernel state in the model. Estimated parameter functions $(a(\alpha), K1(\alpha))$ are fixed, and parameters $(K_{20}(\alpha), K_{21}(\alpha))$ are estimated from large amplitude forced oscillation data by output-error minimization. For GTA, this data is available at three mean $\alpha = (15, 25, 35)$ and three frequencies $f = (0.5, 1, 1.5)Hz$. The response of the estimated model in one case with $\alpha_m = 30\,\text{deg}, \delta\alpha = 25\,\text{deg}$ is shown in Fig. 2. The match is excellent. For pitching moment coefficient three state Volterra variational model gave sufficiently accurate match to the experimental data. Linear part of this model is equivalent to linearized form of other model structures proposed in literature, but this is the first model that provides a systematic approach to model nonlinear variations in coefficients. In nonlinear form, it is also equivalent to the polynomial differential model proposed in [1, 9].

## 2.2 Modeling Abrupt Wing Stall at High Subsonic Mach number

At high-subsonic Mach number and moderate angle-of-attack flight conditions, some aircrafts experience an abrupt asymmetrical wing stall leading to wing-drop or roll-off [2, 3]. This part of the flight envelope is critical for aircraft maneuvering capabilities. The sudden event of roll-off causes degradation of handling qualities and can lead to departure outside the normal flight envelope. If the resulting instability is mild it can be removed by roll-rate feedback in the control law, else it requires an aerodynamic fix on the aircraft.

Free-to-roll (FTR) test is now accepted experimental wind tunnel method for investigation of abrupt wing stall (AWS) along with classical static and unsteady tests. In FTR, the aircraft model has single degree-of-freedom about its roll-axis and can be set at different attitudes specified by pitch angle θ. For GTA, FTR data showed an onset of wing-rock at $\alpha = 26$ deg about a non-zero side-slip at transonic Mach number. There is also an indication of static hysteresis in the rolling moment coefficient versus β at transonic Mach numbers seen from quasi-steady wind tunnel tests. The objective for modeling is to complement model (2), which is capturing only mild nonsingular nonlinearities, with bifurcational properties. A novel bifurcational model of aerodynamic asymmetry (BMAA) splits the rolling moment coefficient into four components, the first three components are from the aero-database, and $Cl_d(t)$ is the incremental effect of aerodynamic asymmetry due to AWS. BMAA for $Cl_d(t)$ is given by the following equations:

$$C_l(\alpha(t), \beta(t)) = C_{l_{st}}(\alpha) + C_{l_p}(\alpha) \cdot p(t)\bar{b}/2V + \quad (6)$$
$$C_{l_\beta}(\alpha) \cdot \beta(t) + C_{l_d}(\alpha(t), \beta(t))$$

$$\begin{aligned}
x &= f(\beta); y = g(C_{l_d}) \quad (7)\\
x_1 &= x\cos(\phi) + y\sin(\phi)\\
y_1 &= -x\sin(\phi) + y\cos(\phi)\\
x_2 &= x\cos(\psi) + y\sin(\psi)\\
\tau\frac{dy}{dt} &= \left(1 - \frac{x_1^2}{a^2} - \frac{y_1^2}{b^2}\right)y + k*x_2
\end{aligned}$$
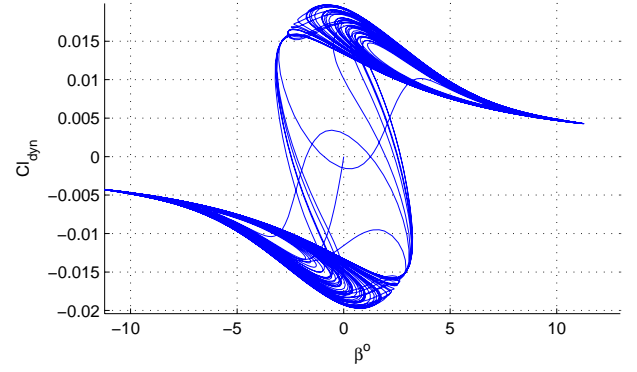


**Fig. 3** Variation of the rolling moment coefficient vs β variation simulated using bifurcational AWS model.

where five parameters $(a, b, k, \phi_m, \psi_m)$ affect the shape of static hysteresis and dynamic properties in steady states. In the hysteresis region there are two stable and one unattainable unstable equilibrium in the center. $C_{l_d}(t)$ triggers rolling motion of the aircraft for $\beta = 0$ to depart to the left or right depending on sign of disturbances. Smooth variation of the rolling moment during the crossing of critical bifurcation points in a dynamic maneuver is due to the first order differential equation with the time-constant τ.

The parameters of the model are estimated in two steps to match FTR data and the rolling moment vs. sideslip from static wind tunnel test data. Parameters $(a, b, k, \phi_m, \psi_m)$ are used to match the shape of steady variation in rolling moment vs. beta static. Time-scale τ is used to match the frequency of oscillation in $\phi(t)$ to that from FTR tests. The model response for GTA with parameters estimated from FTR data is presented in Fig. 3. The model successfully captures the hysteresis in CRM vs. sideslip and dynamic tests on FTR rig. This model is integrated with the aero-database of GTA for simulation. The open-loop simulation model exhibited a mild wing-drop phenomena ultimately leading to wing-rock while performing a steady turn maneuver.

## 3 Nonlinear Flight Dynamics Methodology

Flight simulation technology is now widely used in aeronautical design process and also as an effective platform for pilot and crew training. It is recognised that an adequate aerodynamic model extended beyond normal flight envelope allows one to address flight safety issues both in design and by training. Piloted flight simulation can be made more effective based on clear understanding of aircraft nonlinear dynamics. Note that the analysis methods and computational algorithms for investigation of nonlinear flight dynamics during recent years have improved to a level that computational mathematical model is practically identical to the model used on flight simulator. For a reliable investigation, it is essential that the nonlinear representation of aircraft's dynamics meets the best fidelity level possible through selection of equations of motion, different types of aerodynamic model and representation of control system, etc.

### 3.1 Computational framework

In the present study we rely on computational framework that allows us to conduct comprehensive investigation of aircraft nonlinear dynamics in extended flight envelope using full flight simulation mathematical model without any substantial simplifications. Some elements of this computational framework were presented in [11, 12, 14].

### 3.2 Motion models for various time scales

Aircraft flight dynamics in 6-dof with rigid body approximation can be considered on different time scales. There are three types of fast modes of longitudinal and lateral-directional motion: the Short-period pitching, Dutch roll oscillations and aperiodic roll subsidence. They have a scale of several seconds and can be analysed using assumption that speed of flight is constant and gravity effect is insignificant. Equations called "Spat5" for angle of attack, sideslip and rotation rates in body axes frame $(p, q, r, \alpha, \beta)^T$ were used for evaluation of all attainable trim conditions and their local stability characteristics

for velocity vector roll manoeuvre. Two additional modes of motion associated with variation of flight speed and influence of gravity, phugoid and spiral modes, are much slower, and have roughly ten times higher characteristic time scales. They can be analysed using extended system of equations of motion called "Spat8" with state vector $(p, q, r, \alpha, \beta, V, \theta, \phi)^T$, where $V$ is speed of flight and $\theta, \phi$ are pitch and bank angles respectively. Equilibrium points or trimmed states in this system of equations correspond to a class of helical trajectories with vertical axis of rotation, for example, level flight, horizontal turns, ascending and descending helix trajectories. The full 6-dof simulation is based on "Spat12" system incorporating all twelve states $(p, q, r, \alpha, \beta, V, \theta, \phi, \psi, X, Y, Z)^T$, where $\psi$ is the Euler yaw angle, $X, Y, Z$ are centre of gravity coordinates in the Earth-fixed inertial axes frame.

### 3.3 Open and closed-loop airframes

Flight control system plays significant role in aircraft dynamics. Command and stability augmentation system (CSAS) improves aircraft responses to pilot control inputs and modifies its reaction to external disturbances via change in the short-period, Dutch roll and roll subsidence motion modes. Block-diagram structure of a typical CSAS for longitudinal channels is shown in Fig. 4. It includes dynamic blocks with additional internal states and nonlinear elements that set constraints on the input and output signals, gain scheduling, etc. Similar block-diagram structures are also used for the lateral and directional channels.

The trim and linearization problem for a closed-loop system bears serious difficulties due to much higher dimension and non-smooth nonlinearities. In this work, we use a two tier procedure for this problem as proposed in [14] by the authors. First, the aircraft model is trimmed at a specified manoeuvre. Then open-loop system is linearized at the estimated values of control effectors and model states. In the second step, the control laws are trimmed at these values of model states and deflection of control surfaces. Then the required pilot stick inputs are identified and the
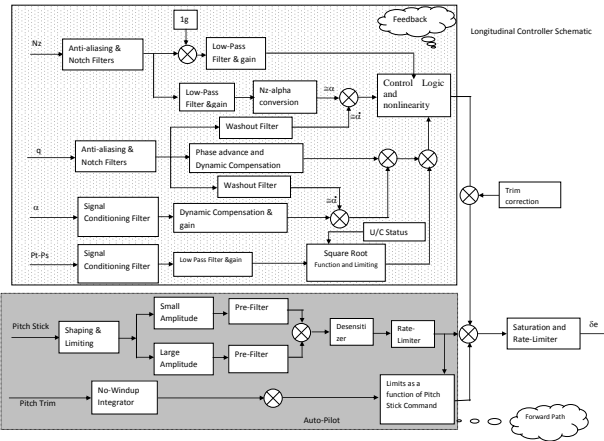
**Fig. 4** Block-diagram of the longitudinal command and stability augmentation control system (CSAS).

control laws are linearized. The open-loop equilibrium state is rejected if the required pilot stick inputs exceed their limits. For attainable trims of the closed-loop system, the linearized matrices of aircrafts states and control laws are augmented to obtain eigenvalues for the closed-loop system. Thus, all the attainable equilibrium states are identified for the open airframe, and then the attainable trims, linearization and system closure are executed using the control law equations.

### 3.4 Flight performance evaluation

Equilibrium states in "Spat8" related to level flight, horizontal turn, etc. characterise aircraft performance characteristics. The eigenvalues of the linearized system describe dynamic properties of the aircraft fast and slow modes of motion. Note that CSAS stabilizes only the fast modes, while phugoid and spiral modes may be left weakly unstable allowing pilot to easily compensate for them. Fig. 5 shows computation of the flight envelope region for a horizontal turn manoeuvre with turn rate $\Omega = 5$ deg/s. The top plot corresponds to the open-airframe having aperiodic instability at low Mach numbers (red points), while the closed-loop system (Fig. 5, middle plot) is stable for all three fast modes of motion in the whole attainable envelope. The bottom plot is visualisation of the level turn. Regions for attainable ascending and de-

scending helical trajectories can be computed in a similar manner with provision of all states and deflections for all control effectors.

Only descending helical trajectories are possible when thrust falls below required level. This trajectory becomes spin when trajectory radius shrinks to the order of several meters. Figure 6 shows examples of one-parametric continuation (Bifurcation diagrams) for equilibrium solutions of "Spat8" system extracted from the computational framework [11]. The top plot presents dependence on elevon at zero aileron setting, and the middle plot shows dependence on aileron at zero elevon setting. Stable equilibrium states are marked in green. Unstable equilibrium states are classified accordingly to distribution of unstable eigenvalues. For example, aperiodically unstable equilibrium with one positive real eigenvalue is marked in red and named as "a1", oscillatory unstable equilibrium with one unstable complex-conjugate pair of eigenvalues is marked in yellow ("o2"), higher order instability is marked by various colors and named accordingly to unstable eigenvalues as "a2", "a1,o2", etc. Graphs in the left column correspond to the open airframe, and those in the right column to the closed-loop system. One can see that CSAS has stabilizing effect only at normal flight conditions with low angles of attack. There are some stabilizing changes for steep spin modes and no qualitative changes for flat spin modes. Time histories in the bottom plot illustrate departure from unstable equilibrium point at high angles of attack to a wing rock attractor. This wing-rock has a quite high periodic time of 30 seconds which allows pilot to apply stabilizing control action.

### 3.5 Flight maneuverability evaluation and control laws clearance using attainable equilibrium sets

The maneuverability metric depends on achievable magnitudes of angle of attack and rate of rotation. These are defined via computation of attainable equilibrium states in the system "Spat5". For execution of a particular maneuver, its equilibrium state in "Spat5" should be stable while its region of attraction be sufficiently large to com-

pensate for probable external disturbances. The CSAS modifies the local stability characteristics and also changes the shape of attainable equilibrium region. Thus maneuverability metric may be confined or extended by a proper choice of control laws. Fig.7 presents attainable equilibrium states for the open airframe and closed-loop system. The open airframe is aperiodically unstable at law angles of attack in the longitudinal mode and oscillatory unstable at high angle of attack in the lateral-directional mode (top plot). Excluding the defined constraints on pilot inputs, the control law stabilizes most of unstable equilibria, leaving unstable sub-regions with reduced level of instability at high rotation rates and high angles of attack (the middle plot). The attainable envelope can be shaped to preserve only stable attainable equilibria via a proper shaping of input signal constraints [14]. Example of such modification is shown in Fig.7 (bottom plot).

Fig.8 (top plot) shows a two-dimensional cross-section of region of attraction computed for a stable equilibrium point of the closed-loop system at high angles of attack (green points). Perturbed motion with initial conditions from all green points in the plane of sideslip and roll rate in Fig.8 (middle plot) converges back to the equilibrium point. Outside of the region of attraction (red points) perturbed motion departs to the auto rotative steep spin regime (Fig.8, bottom plot).

Although the loss-of-control in flight at high angles of attack is possible, the probability of such event depends on the type of flight maneuver, external disturbances and criticality of pilot's control inputs. Fig.9 (top plot) shows spatial maneuver in a form of ascending trajectory with significant reduction in speed and increase in angle of attack (well beyond normal flight envelope) with subsequent successful transition to a normal flight without being attracted by wing rock and spin modes (bottom plot time histories).

## 4    Concluding remarks

The methodological principles and computational framework implemented in this study have provided a deep insight into GTA nonlinear dynamic behaviour in extended flight envelope and allowed to perform effective computational clearance of the flight control laws. A further work is planned with objective of redesign of the flight control laws in extended flight envelope.

## References

[1] Abramov NB, Goman MG, Khrabrov AN et al. Aerodynamic model of transport airplane in extended envelope for simulation of upset recovery. ICAS-2012-3.1.2, *28th International congress of the Aeronautical Sciences*, 23-28 September 2012, Brisbane, Australia, 2012.

[2] Owens SD B, Capone FJ, Hall RM, et. al. Transonic Free-To-Roll Analysis of the F/A-18E and F-35 Configurations *AIAA Atmospheric Flight Mechanics conference*, Providence, Rhode Island, USA, 2004-4053, Aug 2004.

[3] Schuster DM and Byrd JE. Transonic Unsteady Aerodynamics of the F/A-18E under Conditions Promoting Abrupt Wing Stall. *AIAA Journal of Aircraft*, Vol. 41, No. 3, 2004.

[4] Rugh WJ. *Nonlinear System Theory: The Volterra/Weiner Approach*. The John Hopkins University Press, 1981.

[5] Goman MG and Khrabrov AN. State-space representation of Aerodynamic Characteristics of an Aircraft at High-angle-of-attack. *AIAA Journal of Aircraft*, Vol. 31, No. 5, pp 1109-1115, 1994.

[6] Abramov NB, Goman MG and Khrabrov AN. Aircraft Dynamics at High Incidence Flight with Account of Unsteady Aerodynamic Effects, *AIAA Atmosperic Flight Mechanics Conference and Exhibit*, Providence, Rhode Island, USA, AIAA 2004-5274, Aug 2004.

[7] Klein V and Murphy PC. Estimation of Aircraft Nonlinear Unsteady Parameters From Wind Tunnel Data, *NASA-TM 1998-208969*, NASA Langley Research Centre, Hampton, VA, December 1998.

[8] Bommanahal M and Goman M. Nonlinear unsteady aerodynmiac modeling by Volterra variational approach, *AIAA Atmospheric Flight Mechanics Conf*, Paper AIAA 2012-4654, 13-16 Aug, Minneapolis, MN, 2012.

[9] Abramov NB, Goman MG, Greenwell DI and Khrabrov AN. Two-step linear regression method for identification of high incidence unsteady aerodynamic model. Paper AIAA-2001-

4080, *AIAA Atmospheric Flight Mechanics Conference and Exhibit*, 2001.

[10] Pattinson J, Lowenberg MH and Goman MG. Multi-degree-of-freedom wind-tunnel maneuver rig for dynamic simulation and aerodynamic model identification. *Journal of Aircraft*, Vol. 50, No. 2, pp 551-566, 2012.

[11] Goman MG, Zagainov GI and Khramtsovsky AV. Application of bifurcation methods to nonlinear flight dynamics problems *Progress in Aerospace Sciences* Vol. 33, Issue 9, pp 539-586, 1997.

[12] Goman MG, Khramtsovsky AV and Kolesnikov EN. Evaluation of aircraft performance and maneuverability by computation of attainable equilibrium sets. *Journal of guidance control and dynamics*, Vol. 31, No. 2, pp 329-339, 2008.

[13] Kolesnikov EN and Goman MG. Analysis of Aircraft Nonlinear Dynamics Using Non-Gradient Based Numerical Methods and Attainable Equilibrium Sets, *AIAA Atmospheric Flight Mechanics Conf*, Paper AIAA 2012-4406,13-16 Aug, Minneapolis,2012.

[14] Abramov N, Goman M, Kolesnikov EN and Sidoryuk ME. Investigation of Attainable Equilibrium Sets for Clearance of Flight Control Laws. Paper AIAA 2010-491, *48th AIAA Aerospace Sciences Meeting*, 4-7 January 2010, Orlando, Florida, 2010.
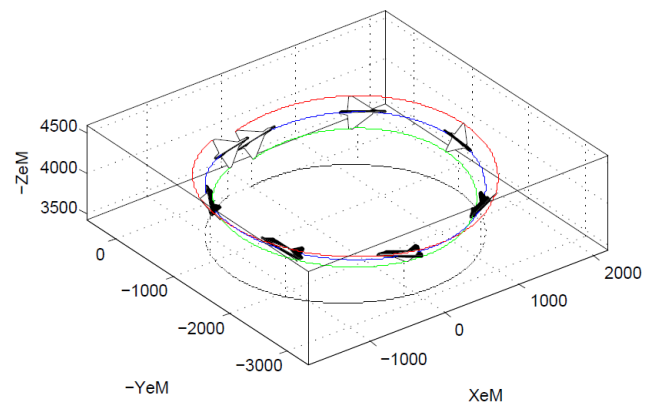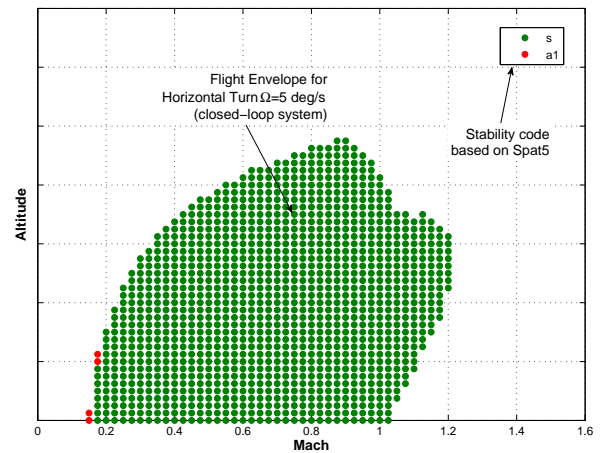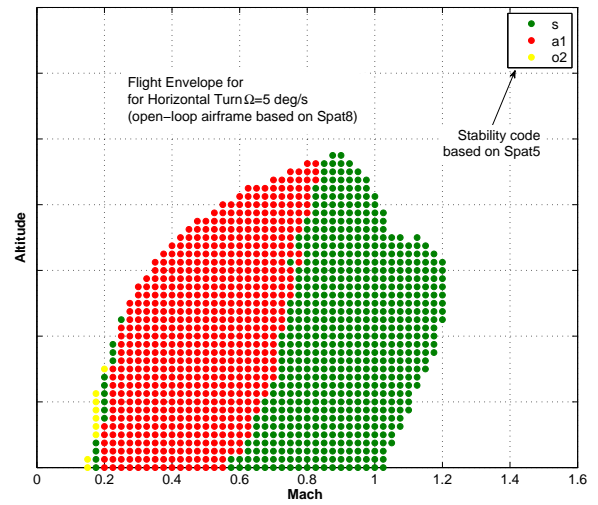
# 5 Contact Author Email Address

Mail to: mgoman@dmu.ac.uk

## Copyright Statement

**Fig. 5** Flight envelope for horizontal turn with yaw rate 5 deg/s computed "Spat8" system: Top plot: open airframe, stability code based on "Spat5" system; Middle plot: - GTA with CSAS, stability code based on "Spat5" system; Bottom plot: visualization of horizontal turn executed at altitude 4000m and Mach number 0.4.
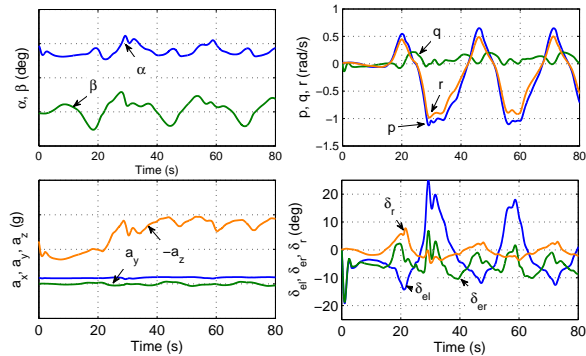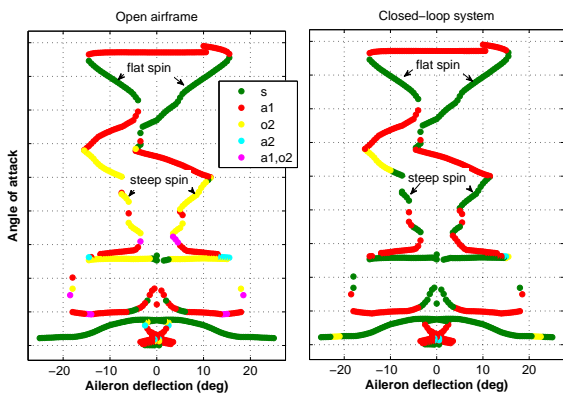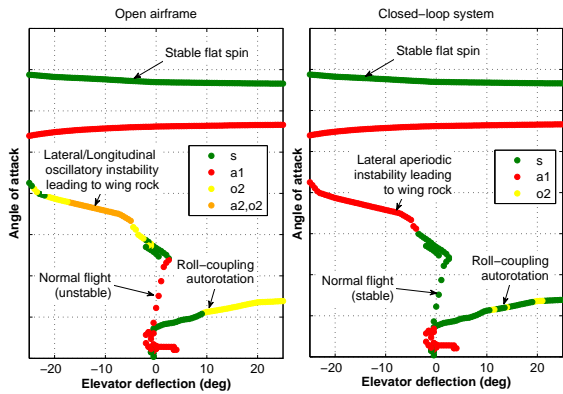
**Fig. 6** Top plot: Dependence of equilibrium angle of attack on elevator at zero aileron and rudder for open airframe and with CSAS computed using "Spat8" system; Middle plot: dependence of equilibrium angle of attack on aileron at zero elevon and rudder for open airframe and with CSAS computed using "Spat8"; Bottom plot: Time histories demonstrating transition of the closed-loop system to wing rock motion from trim angle of attack 39 degrees.
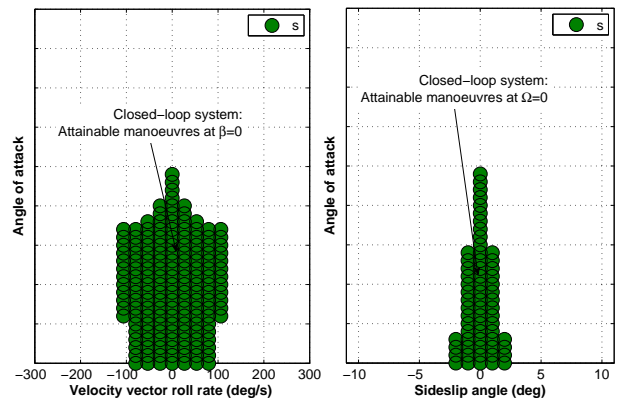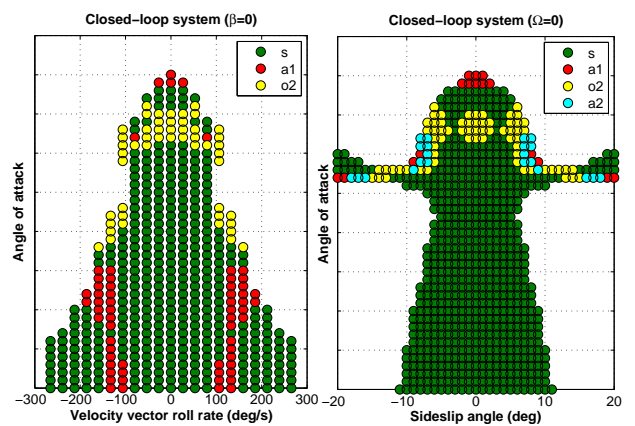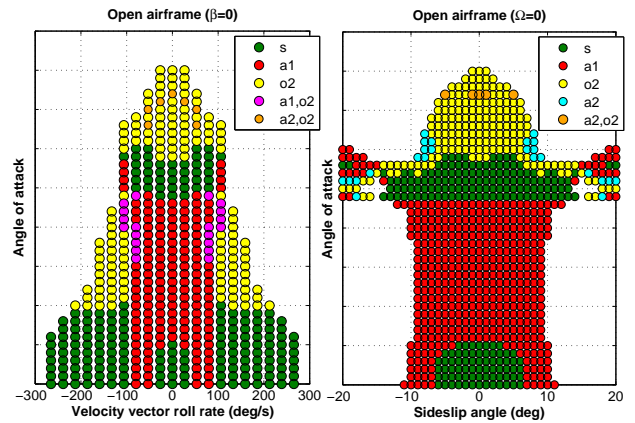
**Fig. 7** Attainable equilibrium sets (AES), cross-sections for zero sideslip and zero roll rate, computed using "Spat5" system for subsonic flight regime Mach 0.4 and altitude 6000m: Top plot: AES for open airframe; Middle plot: AES for airframe with CSAS and no constraints on pilot stick inputs; Bottom plot: AES for airframe with CSAS and imposed constraints on pilot stick inputs.
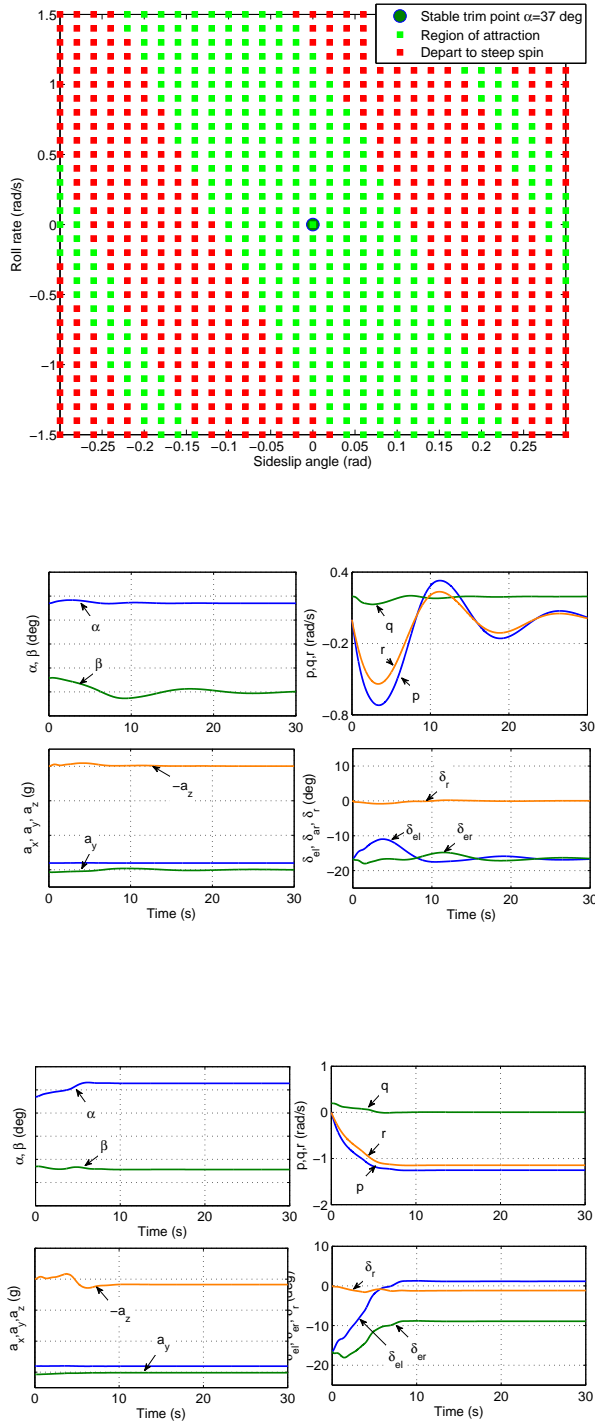
**Fig. 8** Top plot: Region of attraction cross-section $(p, \beta)$ for equilibrium point $\alpha = 37^0$; Middle plot: Process of convergence to the equilibrium point from green points; Bottom plot: Process of departure to the steep spin attractor from red points.
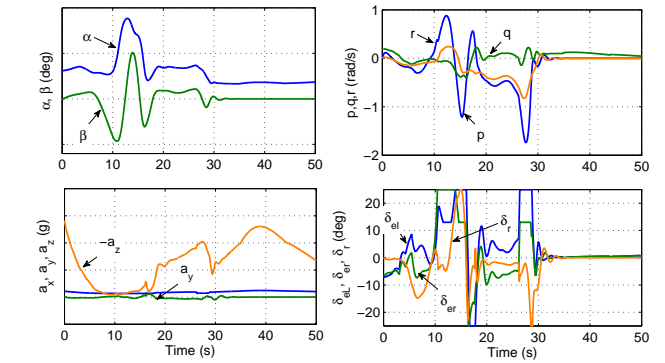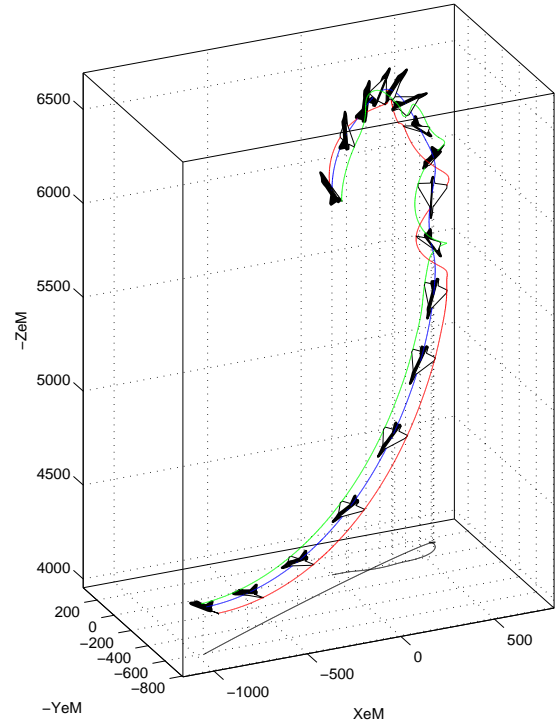
**Fig. 9** Transition through regions of aircrat+CSAS system instability during ascending descending flight trajectory. Top plot: trajectory visualization; Bottom plot: time histories for major state variables and control deflections.